Research Article
Molecular and Cell Biology

JOURNAL
OF HEPATOLOGY

Fetal origin confers radioresistance on liver macrophages via p21$^{cip1/WAF1}$

Graphical abstract

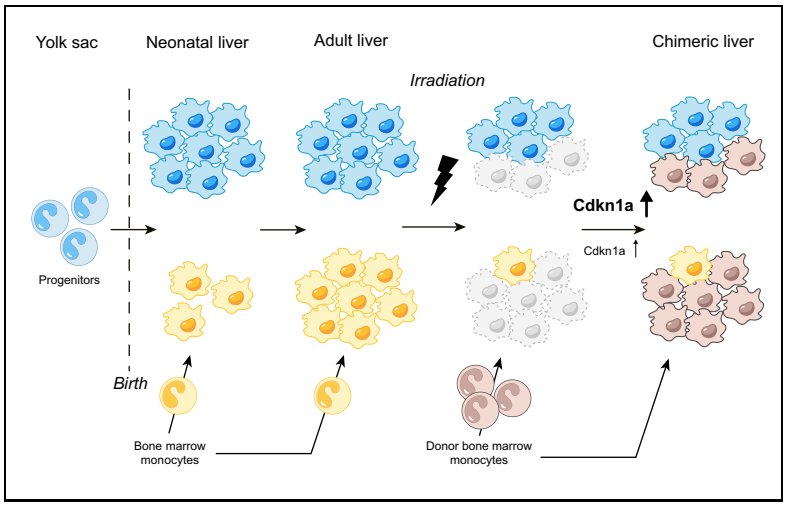

Highlights

- Kupffer cell-specific Cre-driven RiboTag reporter allows translatome analysis.
- Fetal-derived Kupffer cells are relatively radioresistant.
- Adult monocyte-derived Kupffer cells are sensitive to lethal irradiation.
- p21$^{Cip/WAF1}$ regulates the radioresistance of the fetal subset.

Authors

Radika Soysa, Sarah Lampert, Sebastian Yuen, ..., Wanyu Li, Klaus Pfeffer, Ian N. Crispe

Correspondence

soysar@uw.edu (R. Soysa)

Lay summary

Kupffer cells (KCs) are the tissue-resident macrophages of the liver. KCs can be originated from fetal precursors and from monocytes during the fetal stage and post-birth, respectively. Most immune cells in mice are sensitive to lethal-irradiation-induced death, while a subset of KCs resists radiation-induced death. These radioresistant KCs continue to live in the irradiated mice. We discovered that this relatively radioresistant KC subset are the fetal-derived KCs, and they achieve this through cell-cycle arrest. Understanding the radiobiology of KCs will provide valuable insights into the mechanisms that elicit radiation-induced liver disease.

http://dx.doi.org/10.1016/j.jhep.2019.04.015
Published by Elsevier B.V. on behalf of European Association for the Study of the Liver. J. Hepatol. 2019, 71, 553–562

Research Article
Molecular and Cell Biology

JOURNAL OF HEPATOLOGY

Fetal origin confers radioresistance on liver macrophages via p21$^{cip1/WAF1}$

Radika Soysa[1,*], Sarah Lampert[2], Sebastian Yuen[2], Alyse N. Douglass[1], Wanyu Li[3], Klaus Pfeffer[4], Ian N. Crispe[2,5]

[1]*Department of Global Health, University of Washington, Seattle, WA, USA;* [2]*Department of Pathology, University of Washington, Seattle, WA, USA;* [3]*Department of Hepatology, First Hospital of Jilin University, Changchun, China;* [4]*Institute of Medical Microbiology and Hospital Hygiene, Heinrich Heine University, Düsseldorf, Germany;* [5]*Department of Immunology, University of Washington, Seattle, WA, USA*

Background & Aims: Cells of hematopoietic origin, including macrophages, are generally radiation sensitive, but a subset of Kupffer cells (KCs) is relatively radioresistant. Here, we focused on the identity of the radioresistant KCs in unmanipulated mice and the mechanism of radioresistance.

Methods: We employed Emr1- and inducible CX3Cr1-based fate-mapping strategies combined with the RiboTag reporter to identify the total KCs and the embryo-derived KCs, respectively. The KC compartment was reconstituted with adult bone-marrow-derived KCs (bm-KCs) using clodronate depletion. Mice were lethally irradiated and transplanted with donor bone marrow, and the radioresistance of bone-marrow- or embryo-derived KCs was studied. Gene expression was analyzed using *in situ* mRNA isolation via RiboTag reporter mice, and the translatomes were compared among subsets.

Results: Here, we identified the radioresistant KCs as the long-lived subset that is derived from CX3CR1-expressing progenitor cells in fetal life, while adult bm-KCs do not resist irradiation. While both subsets upregulated the *Cdkn1a* gene, encoding p21-$^{cip1/WAF1}$ protein, radioresistant embryo-derived KCs showed a greater increase in response to irradiation. In the absence of this molecule, the radioresistance of KCs was compromised. Replacement KCs, derived from adult hematopoietic stem cells, differed from radioresistant KCs in their expression of genes related to immunity and phagocytosis.

Conclusions: Here, we show that, in the murine liver, a subset of KCs of embryonic origin resists lethal irradiation through *Cdkn1a* upregulation and is maintained for a long period, while bm-KCs do not survive lethal irradiation.

Lay summary: Kupffer cells (KCs) are the tissue-resident macrophages of the liver. KCs can be originated from fetal precursors and from monocytes during the fetal stage and post-birth, respectively. Most immune cells in mice are sensitive to lethal-irradiation-induced death, while a subset of KCs resists radiation-induced death. These radioresistant KCs continue to live in the irradiated mice. We discovered that this relatively radioresistant KC subset are the fetal-derived KCs, and they achieve this through cell-cycle arrest. Understanding the radiobiology of KCs will provide valuable insights into the mechanisms that elicit radiation-induced liver disease.

Introduction

Kupffer cells (KCs), the liver-resident macrophages, are important innate immune sensors that respond to liver stress, and may either stimulate or suppress immunity.[1] In contrast to most other leukocytes, tissue-resident macrophages in the brain (microglia) and epidermis (Langerhans cells) are highly radioresistant.[2,3] However, in the liver, only a subset of KCs resists lethal irradiation, while the other subset is replaced by donor bone-marrow-monocyte-derived KCs (bm-KCs).[4,5] This radioresistant KC subset is long lived, and they are not recruited to foci of inflammation, and thus, are termed sessile KCs.[4,6] Gene expression and epigenetic chromatin modification analysis have confirmed that bm-KCs become broadly similar to sessile KC post-recovery, but not identical.[5,7] While the sessile KC subset is identified post-irradiation, the identity of this subset in unmanipulated mice and why only a subset of KCs resists irradiation are not yet understood.

Kupffer cells traditionally comprise all of the fully mature macrophages in the steady-state liver, identified by F4/80 staining in the mouse. A developing consensus asserts that KCs are a single population of long-lived cells that are seeded from embryonic precursors, and that any other macrophages found in the liver are transient, better-termed "liver macrophages." In favor of this view, several lineage-tracing experiments concluded that all liver-resident macrophages are embryo derived.[8–12] Conversely, other evidence favors the concept that long-lived KCs are heterogeneous, with some derived from blood monocytes. On adoptive transfer into neonates, blood monocytes integrated into the KC niche, indicating that the liver macrophage compartment remained open.[13] Resident fractalkine receptor-1 (Cx3cr1)$^{-hi}$F4/80^{+} subcapsular macrophages are continuously replenished by blood monocytes in the steady-state liver, further supporting the presence of bm-KCs in normal adult liver.[14] A single-cell transcriptome analysis reports two distinct KC clusters based on gene expression *Marco*, *Clec4f*, *Clec1b* versus *Clec4e*, *Clec4d* subsets.[15] While the relationships between subsets identified in these studies are yet to be

Keywords: Cdkn1a; Irradiation; Kupffer cells; Monocytes; RiboTag.
Received 3 January 2019; received in revised form 10 April 2019; accepted 15 April 2019; available online 9 May 2019
* Corresponding author. Address: Department of Pathology, University of Washington, 1959 Northeast Pacific Street, 98195 Seattle, WA, USA.
E-mail address: soysar@uw.edu (R. Soysa).

resolved, a strong case can be made that the liver contains at least two subsets of macrophages: yolk-sac (YS) embryo-derived versus monocyte-derived cells. In this study, we explored the identity of the sessile KC subset in relation to ontogeny, evaluating their embryo versus monocyte origin and potential mechanisms of radioresistance.

Using a combination of fate mapping, radiation chimeras, KC depletion, and *in situ* translatome analysis via the RiboTag mice, we identified the radioresistant sessile KC subset as an embryo-derived, postnatally Cx3cr1-marked F4/80^{-hi} KC subset, and showed that these cells strongly upregulated the *Cdkn1a* gene upon irradiation, and that in the absence of this gene their radioresistance was lost. In contrast, the bm-KC subset was sensitive to irradiation. At the gene expression level, the sessile KCs and the bm-KCs resembled each other, but were not identical, suggesting that these may be functionally distinct subsets.

Materials and methods

Mice

Wild-type (WT; CD45.1, CD45.2), RiboTag (stock number 011029), and *Cx3cr1-CreER* (stock number 021160) mice were purchased from The Jackson Laboratory (CA). All mice were housed in a specific pathogen-free environment. The experiments described were performed under Institutional Animal Care and Use Committee approval. For further details regarding the materials used, please refer to the CTAT table and supplementary information.

RiboTag immunoprecipitation and RNA isolation

The mice were anesthetized with Avertin® (T48402; Sigma, MO). Several liver samples were collected using a 2.0 mm Harris Uni-Core™ (CA), immediately placed in ethanol slurry, and stored at −80 °C until processing. Polysome immunoprecipitation was performed and mRNA isolated, as described by Sanz *et al.*[16]

Cell isolation and flow cytometry

Liver non-parenchymal cell isolation was performed, as described previously.[17] Cells were treated with Fc block (BioLegend, CA) for 10 minutes at 4 °C followed by staining with antibodies for surface antigens at 4 °C for 30 minutes. Intracellular staining was performed on surface-antigen stained cells using Cytofix/Cytoperm™ (BD Biosciences, CA) according to the manufacturer's protocol. Stained cells were analyzed using an LSR II (BD Biosciences, CA) and FlowJo™ software version10.5.0 (FlowJo). Antibodies are listed in Supplementary CTAT table.

Generation of bone-marrow chimeras

Adult mice were lethally irradiated with a single dose of 10 Gy using a Gammacell® 40 Exactor (Best Theratronics, Ontario), and were reconstituted immediately by retro-orbital infusion of 5–7 × 10^6 bone-marrow cells. After 8 or 13 weeks, blood, bone marrow, and liver were assessed for chimerism. In experiments to determine radiation effects over 24 h, the mice were not given bone marrow. In all experiments, control mice that did not receive irradiation received a bone-marrow transplant retro-orbitally except for 24 h experiments.

Tamoxifen inductions

Two-day-old postnatal mice were gavaged with a single dose of tamoxifen, 1 mg (T5648; Sigma, MO) dissolved in corn oil in a total of 50 µl using a 24G-1″ straight 1.25-mm-ball stainless gavage needle (Braintree Scientific, MA). One-week-old mice were gavaged with 1 mg of tamoxifen dissolved in 100 µl, and 6-week-old mice were gavaged with tamoxifen, 2.5 mg dissolved in 200 µl corn oil.

KC depletion

Clodronate or the control liposomes (standard macrophage depletion kit; Encapsula NanoSciences, TN) were injected intraperitoneally to 3-week-old male mice at a dose of 5 mg/20 g body weight in a total of 300 µl to deplete KCs.

Immunofluorescence imaging

Liver pieces were fixed in 4% paraformaldehyde for 12 h, and then transferred to 30% D-glucose and incubated overnight at 4 °C. Samples were optimal cutting temperature (OCT) embedded, cryo-sectioned, and mounted on glass slides. Sections were blocked at room temperature for 1 h with blocking buffer (Triton X-100, 0.02%; bovine serum albumin, 2%; and donkey serum, 5% (Jackson ImmunoResearch, PA), and incubated overnight with primary antibodies, rabbit anti-hemagglutinin (HA) clone SG77 (number 71-5500; Thermo Fisher) at 1:100 and rat anti-mouse F4/80 clone BM8 (BioLegend, CA) at 1:100 dilution in blocking buffer. Sections were washed and incubated with secondary antibodies, donkey anti-rabbit Alexa Fluor® 680, and donkey anti-rat Alexa Fluor 594 (Thermo Fisher) in blocking buffer for 1 h at room temperature. Sections were mounted using DAPI Fluoromount-G® media (SouthernBiotech), and imaged using a Leica TCS SP8 X (Leica, USA) confocal microscopy using 40× objective.

Gene expression analysis

cDNA was generated using the QuantiTect® Reverse Transcription Kit (Qiagen), and pre-amplified using BIO-X-ACT™ Short Mix (Bioline) and the TaqMan® assays of interest (Thermo Fisher, USA). Microfluidic quantitative RT–PCR was performed on a BioMark HD™ microfluidic system (Fluidigm Corp, South San Francisco, CA, USA). The Fluidigm Gene Expression software was used to calculate Ct thresholds, and Microsoft Excel (Microsoft Corporation, Redmond, WA, USA) was used to calculate relative expression levels and fold change value. Gene expression was normalized to *Gapdh* and *Hprt*.

Statistical analysis

Graphs present data from more than three independent experiments. Exact numbers and repetitions are noted in the figure legends. In box and whisker plots, the middle line indicates the median, while bars indicate the minimum to maximum. No randomization or blinding of the investigator was performed. Groups were compared with paired or unpaired Mann-Whitney *U* test with *p* values adjusted for multiple comparisons using Holm-Bonferroni method. Significant *p* values are represented by asterisks ($p > 0.05$). All statistical analyses were performed in either GraphPad Prism 7 or Microsoft Excel (Microsoft Corporation).

Results

RiboTag reporter mice allow *in situ* gene expression analysis of KCs

Current knowledge of gene expression in KCs is based on the analysis of cells isolated using FACS methods, defining them

as the F4/80^{-hi} and CD11b^{+} subset within the CD45^{+} leukocyte population. The efficiency of cell isolation and the purity of KCs are based on the techniques and the surface markers used,[18] emphasizing the difficulty of basing the analysis of KCs exclusively on cells isolated using tissue dissociation.[4,5]

We adopted a strategy first described in neurons[16] to bypass the cell isolation problem and to analyze gene expression via cell-specific activation of the RiboTag reporter followed by polysome immunoprecipitation (RiboIP) (Fig. 1A). To validate the RiboTag approach in KCs, we used Emr1Cre, a Cre driver that uses the promoter from the F4/80 antigen gene.[19] We generated Emr1Cre$^{+/-}$::RiboTag$^{+/-}$ mice, and measured RNAs encoding 140 genes (Fig. 1B; Fig. S2). Tissue-resident macrophage genes identified by the ImmGen consortium[20] (*Emr1*, *MerTK*, and *CD64*) showed over 10-fold enrichment, while the KC-specific gene *Clec4f*[7] and the phagocytosis gene *Marco* were over 50-fold enriched compared to total liver RNA. Phagocytosis genes (*Vsig4* and *Mcr1*) and iron-metabolism-related genes (*CD163* and *Hmox-1*) were also strongly enriched mirroring known functions of steady-state KCs. The analysis of hepatocyte genes (*Alb*, *Hamp1*, and *Cyp2f2*) and sinusoidal endothelial cell genes (*Tie2* and *Lyve1*) indicated a 10-fold or more de-enrichment, while hepatic stellate cell transcript abundance was low in both input and RiboIP fractions. Other myeloid cell genes, such as *Siglecf*, *Ccr2*, *Ly6c*, and *DEC205*, showed only small changes relative to total liver RNA. Similarly, microglia and cardiac macrophages showed enrichment in tissue macrophage genes (Fig. 1E). Immunofluorescence staining using anti-HA and anti-F4/80 antibodies revealed RiboTag stained KCs *in situ* (Fig. 1C). We used intracellular staining of HA protein visualized by flow cytometry to calculate the recombination efficiency. KCs were gated as CD45^{+}, CD11b^{+}, Tie2^{-}, Ly6G^{-}, Siglecf^{-}, and F4/80^{-hi} cells in the live single-cell population (Fig. S1). In Emr1Cre$^{+/-}$::RiboTag$^{+/-}$ mice, ~82% of KCs were labeled with

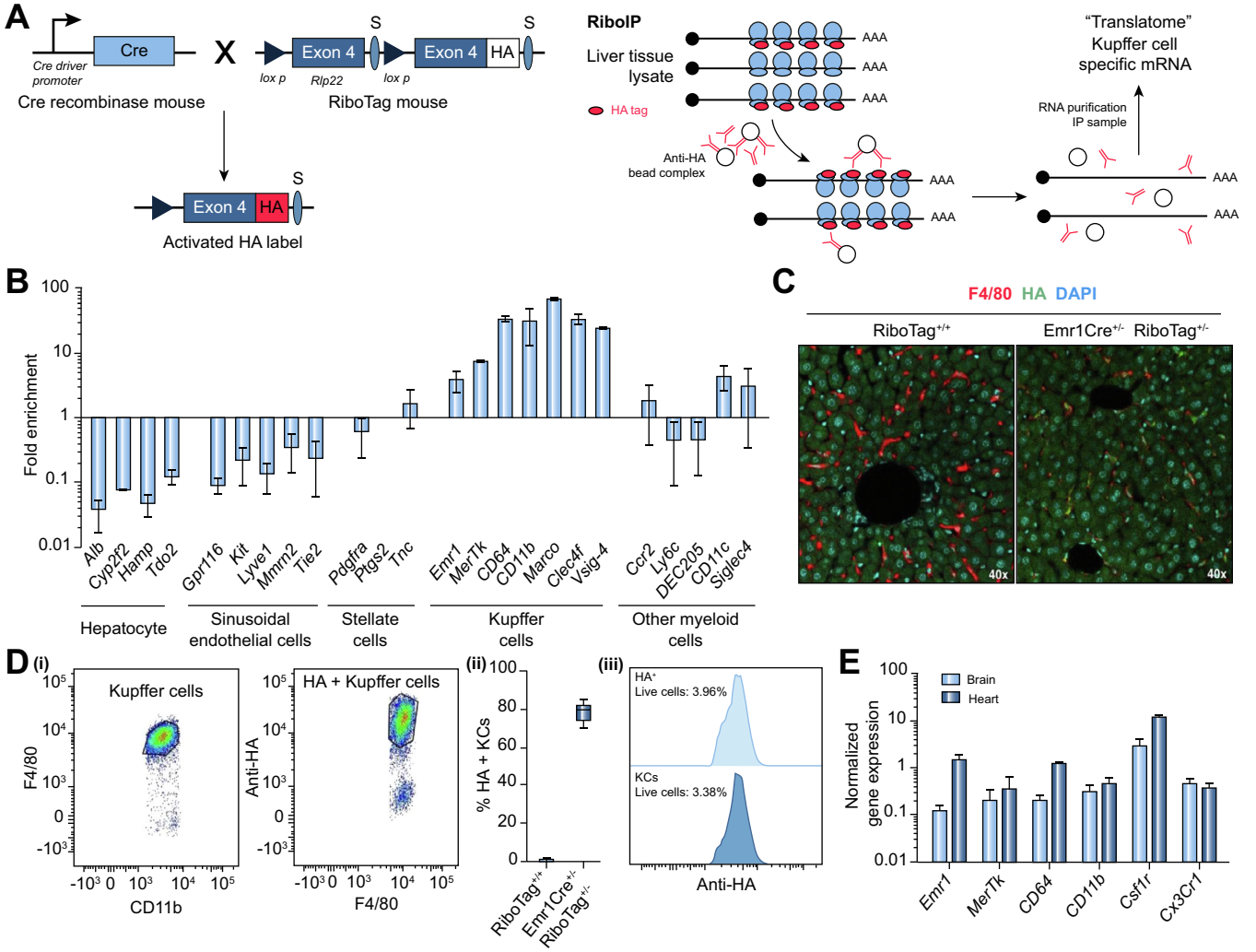

Fig. 1. Emr1Cre-driven RiboTag reporter allows translatome analysis and *in situ* identification of KCs. (A) Diagram illustrates the RiboTag reporter activation by Cre recombinase and the enrichment of cell-specific mRNA in polysome immunoprecipitation (RiboIP). (B) Fold enrichment (IP/input) of KC-associated genes in Emr1Cre$^{+/-}$::RiboTag$^{+/-}$ mice compared to other liver cells. (C) Immunofluorescence images demonstrating the expression of HA antigen–RiboTag (green) on F4/80 (red)-marked KCs in liver sections from RiboTag$^{+/+}$ (left) and Emr1Cre$^{+/-}$::RiboTag$^{+/-}$ (right) mice. Nuclei: cyan (40× magnification). (D) Intracellular FACS analysis showing the proportion of HA-labeled KCs (i), the recombination efficiency of *Emr1*Cre driver in KCs (ii), and the percent HA-labeled cells (green) and the percent KCs (purple) in the live cell population (iii). (E) Gene expression analysis of tissue-resident macrophages in brain and heart of Emr1Cre$^{+/-}$::RiboTag$^{+/-}$ using RiboIP. Data represent three independent experiments with n = 4 mice/group. (B and E) Bars represent the mean ± SD. HA, hemagglutinin; KC, Kupffer cell.

RiboTag, while no other cell subset showed labeling (Fig. 1D). The exclusive labeling of the F4/80^{-hi} cells further confirms the high specificity of Emr1Cre in activating reporters in KCs, as described previously.[21] A recent study used RiboTag mice to define the translatome in microglia.[22] We here extend the use of RiboTag to KCs.

Gene expression in sessile KCs versus bm-KCs

Transcriptomes of sessile KCs versus bm-KCs 8 weeks post-irradiation were defined in KCs isolated using FACS,[5] but we set out to compare their translatomes. We generated radiation bone-marrow chimeras where the *Emr1Cre* and *RiboTag* transgenes were localized to either the sessile KCs or the bm-KCs (Fig. 2A).

Immunofluorescence images distinguished the host versus donor-derived KCs based on HA expression 8 weeks post-irradiation (Fig. 2B). We compared the expression of 94 expressed genes in the two subsets (Fig. 2C; Fig. S4). Characteristic tissue macrophage genes (*Emr1*, *MerTK*, and *CD64*) and phagocytosis-related genes (*Clec4f*, *Vsig4*, and *Msr1*) were expressed to a similar level in both subsets. Among the differentially expressed genes, sessile KCs showed a significantly higher expression of the phagocytosis gene *Marco*, apoptotic cell engulfment gene *Timd4*, c-lectin family scavenger receptor *Colec12*, iron homeostasis gene *Hmox1*, and cell-cycle inhibitor *Cdkn1a*. The bm-KCs showed a significantly higher expression of major histocompatibility complex (MHC) Class II genes (*H2-Ab1* and *H2-Aa*), while the MHC Class I gene (*H2-K1*) was similar in both subsets. While these data are consistent with previous findings on differentially expressed genes in sessile KCs versus bm-KCs,[5] we did not find the hemoglobin scavenger receptor (*CD163*) and erythropoietin receptor (*Epor*) to be different between the two subsets. This may explain the differences between dissociation and FACS versus *in situ* mRNA capture, and the differences between transcriptome versus translatome analysis. A recent study clearly documents the differences in gene expression in microglia in a side-by-side analysis of sorted cell transcriptome versus RiboIP translatomes.[22] Overall, we confirmed that sessile KCs and bm-KCs express many macrophage genes similarly, but some very differently.

Since only the sessile KCs were exposed to irradiation, it is plausible that differential gene expression in this subset was due to the radiation, rather than to distinct subsets. To test this, we compared the gene expression of nonirradiated control mice

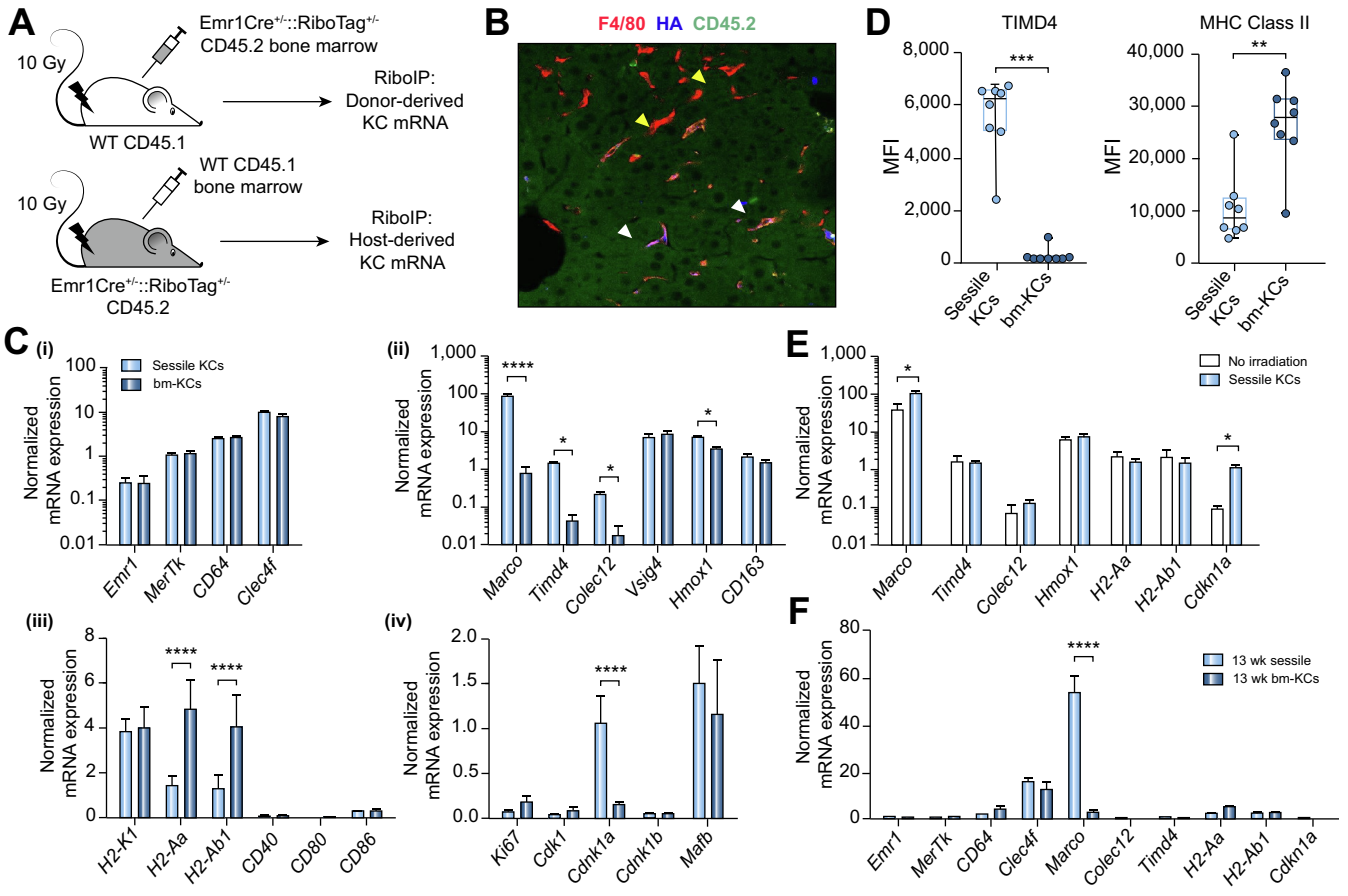

Fig. 2. Gene expression analysis of radioresistant sessile KCs and bm-KCs. (A) Diagram illustrates the generation of radiation chimeras between wild-type and Emr1Cre$^{+/-}$::RiboTag$^{+/-}$ mice. (B) Immunofluorescence image demonstrating the sessile (white arrows) and bm-KCs (yellow arrows) in a radiation chimera, where sessile KCs express RiboTag (blue) and CD45.2 (green). (C) Gene expression analysis of sessile versus bm-KCs at 8 weeks post-irradiation of KC-associated genes (i), phagocytosis and ion-metabolism-associated genes (ii), antigen-presentation-associated genes (iii), and cell-cycle-associated genes (iv). (D) FACS analysis of surface *TIMD4* and MHC Class II protein levels in sessile versus bm-KCs. (E) Radiation-induced gene expression differences in sessile KCs compared to nonirradiated mice at 8 weeks post-irradiation. (F) Gene expression differences at 13 weeks post-irradiation between the sessile KCs and the bm-KCs. Data represent at least three independent experiments with n = 4 mice/group. (D) Indicates MFI. (C, E, and F) Indicate the mean ± SD. $^{*}p \leq 0.05$, $^{**}p \leq 0.01$, $^{***}p \leq 0.001$ (Mann-Whitney *U* test with *p* values adjusted for multiple comparisons using Holm-Bonferroni method). bm-KC, bone-marrow-derived Kupffer cell; HA, hemagglutinin; KC, Kupffer cell; MFI, median fluorescence intensity; WT, wild-type.

to sessile KC subset 8 weeks post-irradiation. In the sessile subset, *Marco* and *Cdkn1a* showed radiation-induced changes in gene expression that persisted up to 8 weeks (Fig. 2E). To determine whether the differential gene expression between sessile KCs versus bm-KCs balanced out over time, we analyzed the gene expression in the sessile KC versus the bm-KC subset 13 weeks post-irradiation. While the level of *Timd4*, *Colec12*, *Hmox1*, *Cdkn1a*, *H2-Ab1*, and *H2-Aa* expressions became comparable by 13 weeks, *Marco* expression remained 40-fold higher in sessile KCs compared to the bm-KC subset (Fig. 2F). Collectively, our results indicate that tissue environment is not the sole driver of gene expression in KCs.

Cx3cr1-based lineage-tracing labels embryo-derived long-lived KCs in the adult liver

While it is clear that a subset of KCs resists irradiation, the origin of this sessile subset in the nonirradiated liver remains unclear. Thus, we labeled the embryo-derived KCs in adult mice using a fate mapping approach.

We devised a RiboTag reporter and inducible Cre recombinase-based strategy to label embryo-derived KCs immediately after birth. *Cx3cr1*-driven tamoxifen-inducible Cre, termed *Cx3cr1CreER*, is used in tissue macrophage lineage tracing.[9,23,24] Developmental studies in embryos indicate that *Cx3cr1* is expressed in YS precursors that give rise to tissue macrophages and maintain expression on microglia and a subset of cardiac macrophages into adulthood.[23–28] However, in KCs, *Cx3cr1* expression ceases after the early postnatal period.[9,23] Furthermore, *Cx3cr1* is also expressed on a subset of dendritic cells and monocytes; thus, a constitutive *Cx3cr1-Cre* driver would not have been truly cell-type specific.

Using FACS, we found that, at neonatal Day 2, only 43% of KCs expressed CX3CR1, while monocytes expressed none (Fig. 3B; Fig. S5). This indicates that, by Day 2, at least 43% of embryo-derived KCs continued to express *Cx3cr1*, while it is possible that some had already ceased expression. Furthermore, the absence of CX3CR1^{+} monocytes suggested that CX3CR1^{+} monocyte-derived macrophages were not seeding the liver within the first 2 days. Thus, the first 2 days after birth provide a window to label embryo-derived KCs using the tamoxifen-inducible *Cx3Cr1-eyfp-CreER* model. We bred *Cx3cr1-eyfp-CreER*$^{+/+}$ mice with RiboTag$^{+/+}$ mice, and the offspring were tamoxifen induced within the first 2 days of birth (Fig. 3A). At 8 weeks, we analyzed the liver tissue by immunofluorescence,

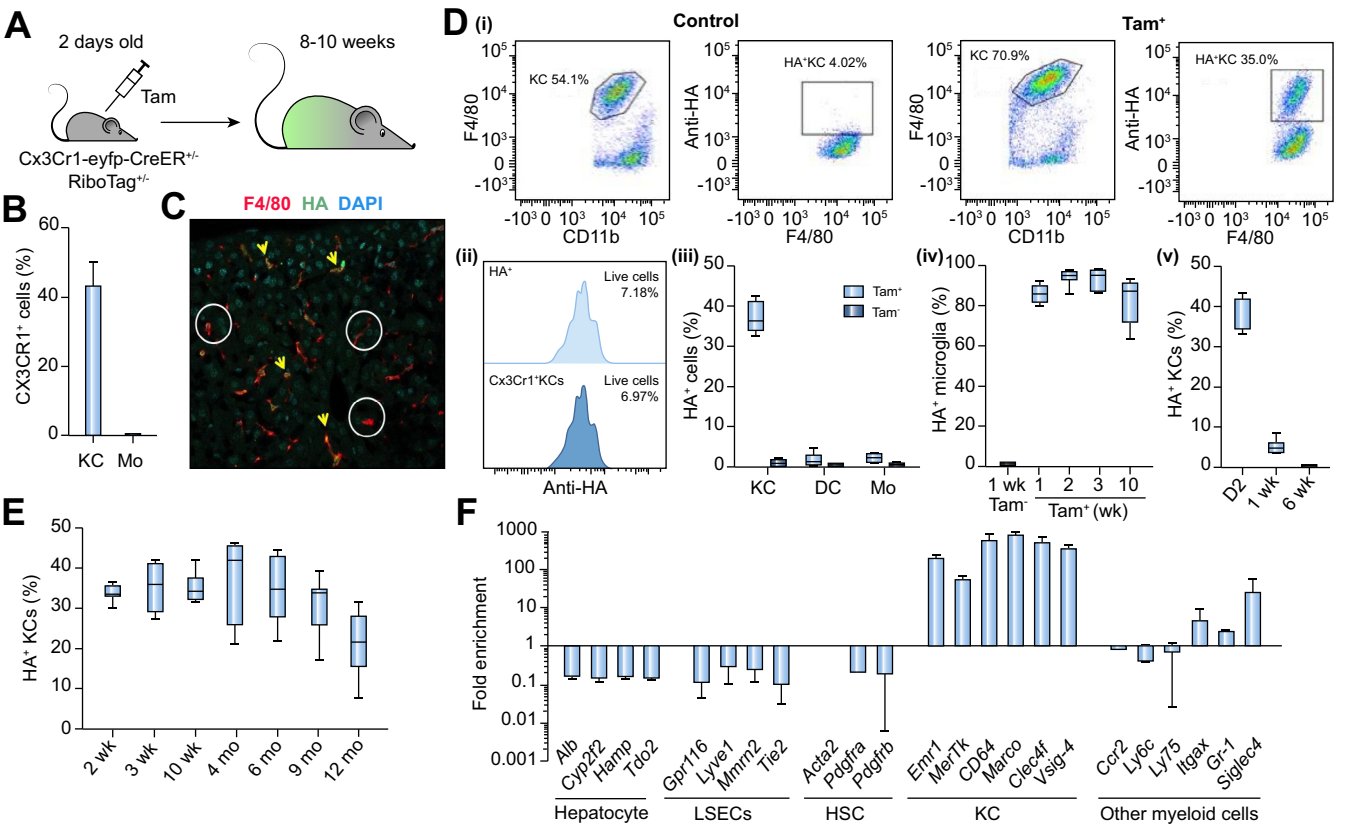

Fig. 3. Cx3cr1-based fate mapping labels embryo-derived long-lived KCs in the adult liver. (A) Diagram illustrates the irreversible labeling of KCs within the first 2 days of birth in *Cx3cr1-eyfp-CreER*$^{+/-}$*::RiboTag*$^{+/-}$ mice following tamoxifen administration. (B) Percent cells expressing CX3CR1 in KCs and monocytes in 2-day-old mice determined by FACS. (C) Immunofluorescence image of adult mouse liver, post-D2 tamoxifen induction, indicating the presence of F4/80^{+} KCs (red) and HA antigen (green). Yellow arrows: postnatally Cx3cr1-marked KCs; white circles: non-labeled KCs. (D) Intracellular FACS analysis of adult mice post-Day 2 tamoxifen induction compared to the control showing the RiboTag-labeled KCs (i); the percent HA-labeled and Cx3cr1-marked KCs in the live cells (ii); the percent HA labeling in liver KCs, DCs, and MO (iii); the percent HA-labeled microglia following Day 2 induction (iv); and the percent HA-labeled KCs in 10-week-old mice following tamoxifen induction at 2 days, 1 week, or 6 weeks (v). (E) Following 2 days tamoxifen induction, Cx3cr1-labeled KC turnover up to 12 months analyzed using FACS. (F) Fold enrichment of KC-associated genes. Data represent >3 independent experiments with n >5 mice/group. (B and F) Bars indicate the mean ± SD. DC, dendritic cell; HA, hemagglutinin; HSC, hematopoietic stem cell; KC, Kupffer cell; LSEC, liver sinusoidal endothelial cell; MO, monocyte.

and showed that only a subset of KCs was labeled with RiboTag (Fig. 3C). Intracellular FACS staining showed that 37% of the total KCs in the adult mice were RiboTag labeled, hence, were postnatally Cx3cr1 marked, representing the embryo-derived KC subset (Fig. 3D, i and ii). In contrast, microglia showed ~80% RiboTag labeling indicating that the labeling efficiency of *Cx3cr1-eyfp-CreER* promoter was about 80% (Fig. 3D, iv). FACS analysis further revealed that monocytes or dendritic cells in the adult liver did not carry RiboTag labeling, indicating that any cell that was labeled in the early postnatal period had turned over by 8 weeks (Fig. 3D, ii).

Labeling at 1 and 6 weeks, and analysis at 10 weeks of age showed labeling reduced to only 2% and <1%, respectively (Fig. 3D, v), providing further evidence that the *Cx3cr1* expression ceased on embryo-derived KCs early in development, and that the Cx3cr1 fate-mapping strategy could be only used to label embryo-derived KCs within the first days after birth. To determine the turnover of Cx3cr1-marked KCs in the liver, we measured the frequency of HA+ KCs at 2, 3, and 10 weeks and 4, 6, 9, and 12 months post-induction among the total KCs in mice induced on neonatal Day 2. The Cx3cr1-marked KCs maintained a 37% frequency among total KCs up to 9 months before declining to 22% by 12 months (Fig. 3E), showing their stability over time. This observation is consistent with a previous report that postnatally labeled KCs survived up to 9 months;[23] however, our data suggest these were more abundant than the previously reported 7%.

Next, we examined gene expression in the Cx3cr1-marked KCs, and showed that consensus tissue macrophage genes (*Emr1*, *MerTK*, and *CD64*) and KC-related genes (*Marco* and *Clec4f*) were highly enriched, while hepatocyte, sinusoidal endothelial cells, hepatic stellate cells, and other myeloid markers were either de-enriched or showed no change (Fig. 3F; Fig. S2). Taken together, these data show that *Cx3cr1-eyfp-CreER* combined with RiboTag fate mapping allows both labeling and gene expression analysis of Cx3cr1-marked embryo-derived KCs following postnatal tamoxifen induction.

Embryo-derived Cx3cr1-marked KCs resist irradiation and express sessile KC genes

To determine whether the Cx3cr1-marked KCs resist lethal irradiation, we generated radiation chimeras in Cx3cr1-marked KC bearing *Cx3Cr1-eyfp-CreER*$^{+/-}$*::RiboTag*$^{+/-}$ mice (Fig. 4A). Eight weeks post-irradiation immunofluorescence analysis of frozen sections clearly indicated the HA label bearing Cx3cr1-marked KCs that persisted after irradiation (Fig. 4C).

Intracellular FACS analysis indicated that 19% of the host-derived KCs in the irradiated group, and 26% of the KCs in the nonirradiated control group were composed of Cx3cr1-marked KCs (Fig. 4D). These results indicate that Cx3cr1-marked embryo-derived KCs were relatively radioresistant. Furthermore, there is a subset of non-labeled host-derived KCs that also resisted irradiation. It is possible that these represent embryo-derived KCs that did not label after they ceased to express *Cx3cr1*. Next, we compared the gene expression of Cx3cr1-marked radioresistant KCs to the sessile KCs, and found that, at the gene expression level, the two subsets closely resembled each other (Fig. 4E). The genes that showed elevated expressions in the sessile subset (*Marco*, *Timd4*, *Colec12*, and *Cdkn1a*) compared to the bm-KC subset were equally elevated in the radioresistant Cx3cr1-marked KCs. These observations

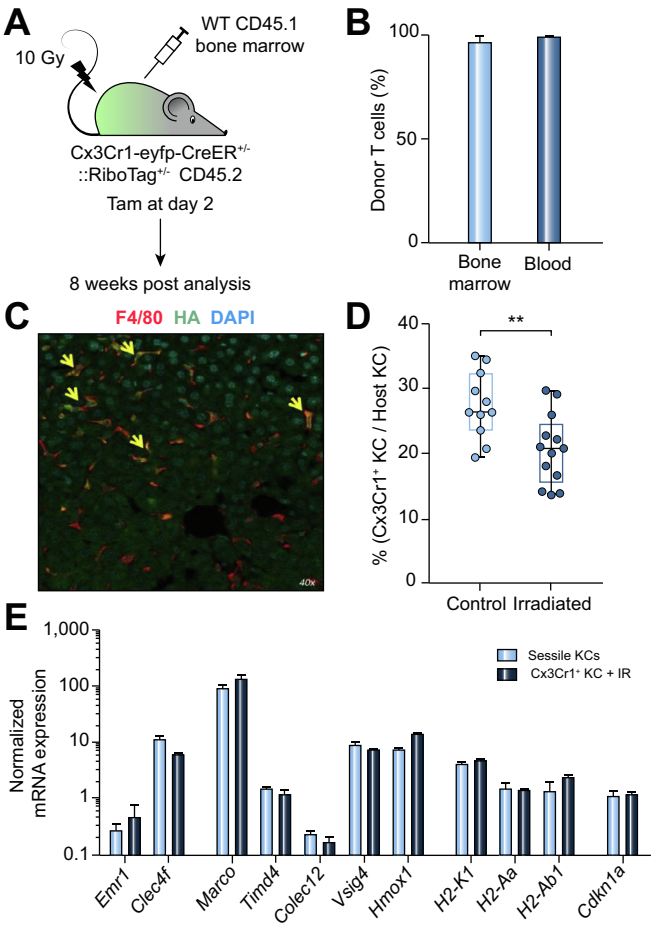

Fig. 4. Embryo-derived Cx3cr1-marked KCs survive lethal irradiation and express sessile KC genes. (A) Diagram illustrates the generation of the irradiation chimera in adult mice with Cx3cr1-marked KCs. (B) Percent donor T cell chimerism 8 weeks post-irradiation and bone-marrow transplant. (C) Immunofluorescence image demonstrating the radioresistant Cx3cr1-marked embryo-derived KCs (yellow arrows) in the chimeric liver 8 weeks post-irradiation. Red: F4/80; green: HA antigen; cyan: nucleus. (D) FACS analysis of the percent Cx3cr1-marked KCs among the total host KCs in irradiated mice compared to nonirradiated controls 8 weeks after irradiation. (E) Gene expression comparison between sessile KCs and embryo-derived Cx3cr1^{+} KCs 8 weeks post-irradiation. Data represent >3 independent experiments with n = 3 mice/group. (B) and (E) bars indicate the mean ± SD. Red dots: individual mice. $^{**}p \leq 0.01$; Mann-Whitney *U* test; IR: 10 Gy irradiation; Cx3cr1+: Day 2 tamoxifen-induced Cx3cr1-marked KCs. HA, hemagglutinin; KC, Kupffer cell; WT, wild-type.

demonstrate that the sessile KCs consist of Cx3cr1-marked, embryo-derived, long-lived KCs.

Bone-marrow-monocyte-derived KCs are sensitive to lethal irradiation

A subset of Cx3cr1-marked embryo-derived KCs both resists irradiation and resembles sessile KCs in gene expression, but we cannot yet rule out the possibility that the long-lived bm-KCs also resist irradiation. A KC depletion–repopulation study indicated that the repopulated KCs were long lived and closely resembled the replaced resident KCs,[13] so it is possible that these bm-KCs were also able to resist irradiation and formed part of the sessile subset. Thus, we next explored whether the bm-KCs also resist irradiation.

Clodronate liposomes effectively deplete all KCs.[29] Immediately after the administration of Clodronate, all F4/80^{-hi} KCs

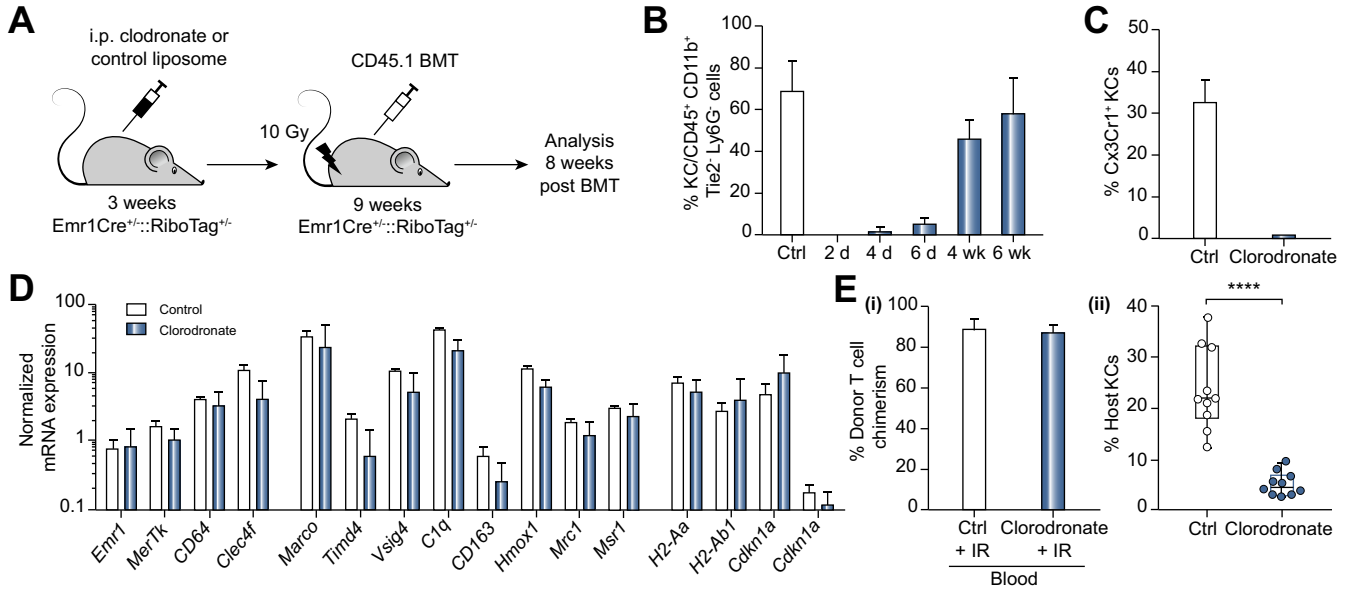

Fig. 5. bm-KCs are sensitive to irradiation. (A) Diagram illustrates the clodronate depletion of resident KCs and radiation chimera generation in Emr1Cre$^{+/-}$::RiboTag$^{+/-}$ mice. Control mice received liposomes without clodronate. (B and C) FACS analysis of depletion–repopulation kinetics of (B) resident KCs, and (C) embryo-derived Cx3cr1-marked (Cx3cr1^{+}) KCs following clodronate treatment compared to controls. (D) Gene expression analysis of KC-associated genes in control and clodronate-treated mice 6 weeks post-administration. (E) Percent donor T cell chimerism (i) and percent host KCs in control and clodronate-treated mice 8 weeks post-irradiation, determined by FACS (ii). Data represent three independent experiments with n >3 mice/group. (B)–(E) bars indicate the mean ± SD. Dots: individual mice. ****$p \leq 0.0001$; Mann-Whitney *U* test; IR: 10 Gy irradiation. BMT, bone marrow transplant; i.p., intraperitoneal; KC, Kupffer cell.

are lost, and over time, blood monocytes differentiate into F4/80^{int} macrophages that will slowly morph into F4/80^{-hi} KCs.[30] To generate a KC compartment solely derived from bone-marrow monocytes harboring the RiboTag reporter, we administered Clodronate into 3-week-old Emr1Cre$^{+/-}$::RiboTag$^{+/-}$ mice (Fig. 5A). The time course confirmed that KCs were totally ablated within 48 h, but restored to ~58% compared to the ~78% control levels by 6 weeks post-Clodronate (Fig. 5B; Fig. S6).

To exclude the possibility of KC repopulation through local proliferation of progenitors, we administered Clodronate into Cx3cr1-marked KC bearing mice at 3 weeks and analyzed at 6 weeks posttreatment. Cx3cr1-marked KCs were completely ablated in the Clodronate group, while there was no effect in the control liposome-treated group (Fig. 5C). This confirmed that, following Clodronate treatment, the repopulation of KCs only occurs from monocyte differentiation, and not from clonal expansion of long-lived resident KCs. Gene expression analysis 6 weeks posttreatment revealed that both Clodronate and control liposome groups show similar level of expression in a panel of 46 genes (Fig. 5D).

To explore the radiosensitivity of these bm-KCs, we lethally irradiated either the Clodronate or the control liposome-treated Emr1Cre$^{+/-}$::RiboTag$^{+/-}$ mice 6 weeks after liposome treatment, and reconstituted with WT CD45.1 bone marrow (Fig. 5A). Eight weeks posttransplant, we analyzed the donor versus host chimerism in blood and liver KCs (Fig. 5E). Clodronate-treated mice had a significantly lower number of host KCs (<5%) compared to the control liposome-treated mice (~25%), suggesting that bm-KCs are sensitive to lethal irradiation. These data clearly indicate that bm-KCs do not contribute significantly to the radioresistant sessile KC subset.

Immediate response of Cx3cr1-marked long-lived sessile KCs and bm-KCs to radiation injury

Next, we set to explore the mechanisms that confer this unique radioresistance on the Cx3cr1-marked sessile KC subset. A recent study indicates that embryo-derived Langerhans cells resist irradiation through a *Cdkn1a*-mediated pathway, while bone-marrow-derived dermal dendritic cells undergo apoptotic death upon irradiation.[31] This could suggest that an embryonic origin confers radioresistance on multiple myeloid lineages. Thus, we next explored the responses of the two KC subsets to irradiation following 24 h.

First, we assessed radiation-induced damage in Cx3cr1-marked embryo-derived KCs versus repopulated bm-KCs after Clodronate treatment. Using intracellular staining and FACS, we detected phosphorylated histone variant γ-H2AX protein, a marker of DNA double-strand breaks,[32] at 24 h after lethal irradiation. The two KC subsets showed similar (>2-fold) upregulation of the γ-H2AX protein, indicating that both subsets were equally susceptible to γ-irradiation-induced double-strand breaks (Fig. 6A).

Next, we compared the expression of genes in the two subsets 24 h post-irradiation. We analyzed the gene expression in 92 genes that were previously implicated in the radiation response, inflammation, macrophage functions, and in cell death versus survival (Fig. 6; Fig. S7).[33–35] Both subsets showed a significant upregulation of p53-dependent radiation-induced genes (*Phlda3*, *Mdm2*, *Sens2*, and *Cdkn1a*), while the antioxidant gene *Nrf2* was also elevated. Cell-cycle progression genes (*Cdk1* and *Ki67*) were downregulated in both groups, indicating cell-cycle arrest (Fig. 6C; Fig. S8). Interestingly, the *Cdkn1a* upregulation in Cx3cr1-marked KCs was 2.5 times higher than in bm-KCs (Fig. 6B). We further confirmed the elevated expression of

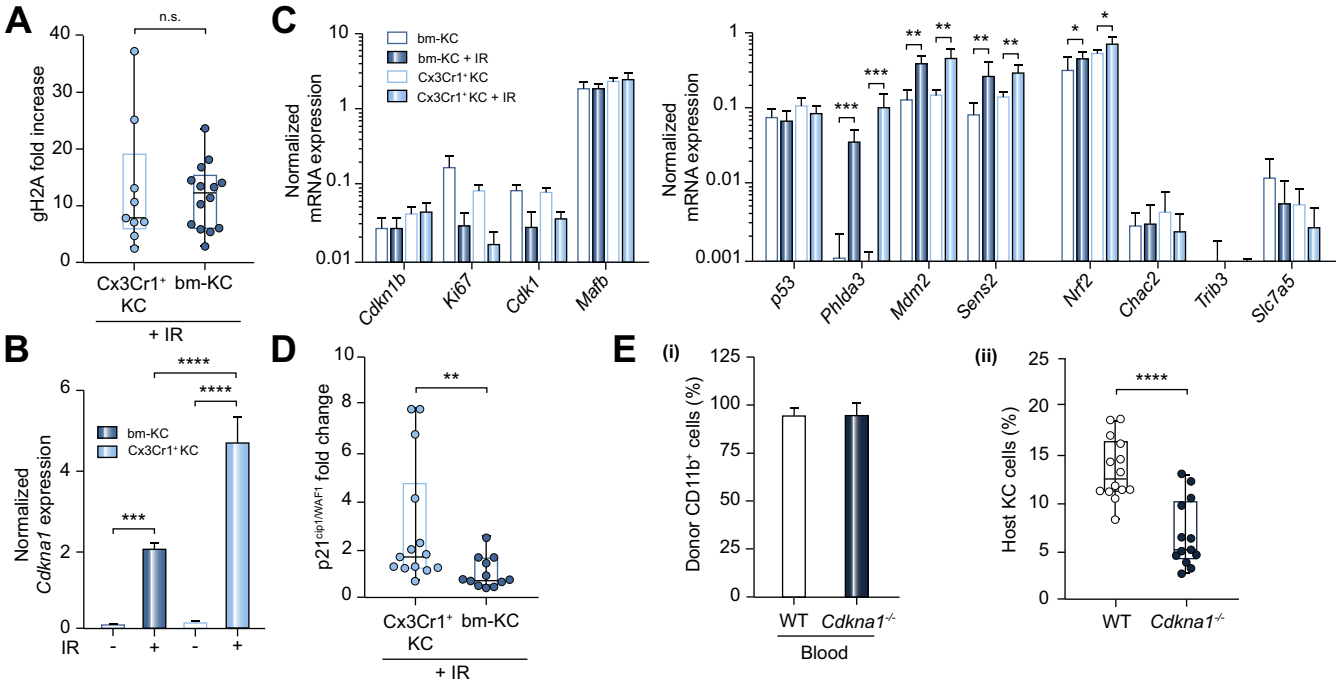

Fig. 6. Immediate response of Cx3cr1-marked sessile KCs and bm-KCs to irradiation. (A) Comparison of γ-H2AX protein fold change compared to nonirradiated controls 24 h post-irradiation in bm-KCs versus Cx3cr1-marked KCs using FACS analysis. (B and C) Gene expression analysis of cell-cycle-associated- and radiation-induced genes. (D) Cell-cycle inhibitor $p21^{Cip1/WAF1}$ protein fold change compared to nonirradiated control mice determined by FACS. (E) Donor $CD11b^+$ chimerism in blood (i), and percent host-derived KCs (ii) determined using FACS 8 weeks post-irradiation. Data represent at least three independent experiments with n >3 mice/group. (C) and (E, i) bars indicate the mean ± SD. Dots: individual mice. $^{**}p \leq 0.01$,$^{****}p \leq 0.0001$. (A, B, D, and E, ii) Mann-Whitney *U* test with *p* values adjusted for multiple comparisons using Holm-Bonferroni method. IR: 10 Gy irradiation; $Cx3cr1^+$ KC: Day 2 tamoxifen-induced Cx3cr1-marked KC. bm-KC, bone-marrow-derived Kupffer cell; KC, Kupffer cell; ns, not significant, WT, wild-type.

$p21^{cip-1/WAF1}$ protein in Cx3cr1-marked KCs by flow cytometry (Fig. 6D).

We hypothesized that the increased upregulation of *Cdkn1a* provides a survival advantage to the embryo-derived KCs. To test this hypothesis, we generated radiation chimeras in *Cdkn1a*–/– mice and WT mice. Eight weeks post-lethal irradiation and congenic bone-marrow transfer, we analyzed the abundance of sessile KCs in each group of chimeras (Fig. 6E). This experiment revealed that the *Cdkn1a*–/– group had two-thirds fewer sessile KCs compared to the control group. Overall, these experiments confirmed that elevated upregulation of the *Cdkn1a* gene and its protein product, $p21^{cip1/WAF1}$, in Cx3cr1-marked KCs results in improved survival of radiation-induced damage.

Discussion

Here, we investigated the identity of sessile KCs and their mechanism of radioresistance. These cells corresponded to a postnatally Cx3cr1-marked embryo-derived subset. In contrast to bm-KCs, the Cx3cr1-marked subset showed a greater increase in *Cdkn1a* mRNA and $p21^{cip1/WAF1}$ protein following irradiation. In the absence of *Cdkn1a*, the sessile KCs significantly lost the ability to survive irradiation, indicating that the enhanced upregulation of *Cdkn1a* provided greater survival potential to the Cx3cr1-marked subset.

Our postnatal labeling strategy consistently labeled at least a subset (∼37%) of the YS-derived KCs based on their continued expression of Cx3cr1. While YS-derived KCs are products of erythromyeloid progenitors (EMPs), the bm-KCs are products of hematopoietic-stem-cell (HSC)-derived monocytes. This suggests that the KCs that originated from HSCs are predisposed to radiation-induced death, while radioresistance is a feature of YS EMP-derived KCs. While a recent report that concluded YS-derived KCs are partially ablated in response to irradiation,[5] we argue that, nevertheless, these cells are relatively radioresistant compared to bm-KCs. While our study does not directly identify these early HSC-derived long-lived KCs, radiation experiments strongly suggest the existence of a YS-derived and an HSC-derived KC subset. This conclusion may be more general, since microglia that are solely derived from YS EMPs are also radioresistant.

The $p21^{-cip1/WAF1}$ protein is a p53-induced molecule that exerts G1 cell-cycle arrest in the context of radiation damage, which may lead to cellular senescence or apoptosis.[36,37] However, $p21^{-cip1/WAF1}$ expression may also be regulated by p53-independent mechanisms, and in this context, it is involved in promoting cell survival.[33,38–40] In our study, the upregulation of $p21^{-cip1/WAF1}$ in both subsets within 24 h of irradiation conforms to the well-known p53-dependent radiation response. However, it is possible that the 2.5 times higher level of *Cdkn1a* gene expression in the Cx3cr1-marked subset compared to bm-KCs is due to p53-independent pathways, and this elevation confers radioresistance on the Cx3cr1-marked subset. While *Cdkn1a* expression decreased by 1 week post-irradiation in Cx3Cr1-marked KCs, it remained significantly high in the sessile subset compared to nonirradiated controls for at least 8 weeks post-irradiation, further suggesting a pro-survival role for $p21^{-cip1/WAF1}$ in this subset (Fig. S8).

Expression of the *Marco* gene remained 40-fold higher out to at least 13 weeks in the sessile subset compared to bm-KCs. Interestingly, when resident KCs were completely depleted,

the repopulating bm-KCs showed a similar level of *Marco* expression to the resident KCs. One possible explanation is that the bm-KCs assume distinct transcriptional patterns during repopulation of a completely versus a partially empty niche. This suggests the existence of two distinct niches, where one is occupied by the sessile KCs and the other by bm-KCs. It is interesting that clodronate depletion creates short-lived gaps in the sinusoidal layer, suggesting that a subset of KCs may be integrated into the endothelium.[41] Based on the restoration of *Marco* gene expression in bm-KCs post-clodronate, we suggest a model, in which YS-derived KCs occupy these intra-endothelial niches early in ontogeny, which directs their distinctive gene expression, including high *Marco* expression. In emergency repopulation after irradiation, these niches remain occupied by YS-derived sessile KCs, but after total KC depletion, the niches are occupied by bm-KCs, which adopt some of the properties of the former occupants.

Human livers also contain a subset of long-lived sessile KCs that persists after transplantation,[42] but the origin of these cells is unknown. The single-cell transcriptome analysis of human liver indicates two distinct subsets of macrophages based on *MARCO* expression, and gene expression suggests that they have pro-inflammatory versus anti-inflammatory functions.[43] Whether the *Marco*^{hi} sessile KCs are equivalent to the *MARCO*$^{+}$ human KCs is yet to be determined.

Financial support

This work was supported by the American Heart Association (award 17PRE33410275to RS), the National Institutes of Health (grant 1R21AI114827 to INC), and the German Research Foundation (DFG) (grant SFB974 to KP).

Conflict of interest

The authors declare no competing interests.

Please refer to the accompanying ICMJE disclosure forms for further details.

Authors' contributions

RS, SL, SY, AND, and WL performed the experiments. KP created the Emr1-Cre transgenic mice and gave input into the experimental protocols. RS and INC designed the study and wrote the manuscript.

Acknowledgements

The authors thank the K-wing vivarium, W. M. Keck Microscopy Center, and the Department of Pathology Flow Cytometry laboratory at the University of Washington for technical support.

Supplementary data

Supplementary data to this article can be found online at https://doi.org/10.1016/j.jhep.2019.04.015.

References

Author names in bold designate shared co-first authorship

[1] Abdullah Z, Knolle PA. Liver macrophages in healthy and diseased liver. Pflugers Arch 2017;469:553–560.
[2] Ginhoux F, Lim S, Hoeffel G, Low D, Huber T. Origin and differentiation of microglia. Front Cell Neurosci 2013;7:45.
[3] Bogunovic M, Ginhoux F, Wagers A, Loubeau M, Isola LM, Lubrano L, et al. Identification of a radio-resistant and cycling dermal dendritic cell population in mice and men. J Exp Med 2006;203:2627–2638.
[4] Klein I, Cornejo JC, Polakos NK, John B, Wuensch SA, Topham DJ, et al. Kupffer cell heterogeneity: functional properties of bone marrow derived and sessile hepatic macrophages. Blood 2007;110:4077–4085.
[5] Beattie L, Sawtell A, Mann J, Frame TCM, Teal B, de Labastida Rivera F, et al. Bone marrow-derived and resident liver macrophages display unique transcriptomic signatures but similar biological functions. J Hepatol 2016;65:758–768.
[6] McDonald B, Kubes P. Innate immune cell trafficking and function during sterile inflammation of the liver. Gastroenterology 2016;151:1087–1095.
[7] **Lavin Y**, **Winter D**, Blecher-Gonen R, David E, Keren-Shaul H, Merad M, et al. Tissue-resident macrophage enhancer landscapes are shaped by the local microenvironment. Cell 2014;159:1312–1326.
[8] **Schulz C**, **Gomez Perdiguero E**, Chorro L, Szabo-Rogers H, Cagnard N, Kierdorf K, et al. A lineage of myeloid cells independent of Myb and hematopoietic stem cells. Science 2012;336:86–90.
[9] **Yona S**, **Kim KW**, **Wolf Y**, Mildner A, Varol D, Breker M, et al. Fate mapping reveals origins and dynamics of monocytes and tissue macrophages under homeostasis. Immunity 2013;38:79–91.
[10] Gomez Perdiguero E, Klapproth K, Schulz C, Busch K, Azzoni E, Crozet L, et al. Tissue-resident macrophages originate from yolk-sac-derived erythro-myeloid progenitors. Nature 2015;518:547–551.
[11] Hoeffel G, Chen J, Lavin Y, Low D, Almeida FF, See P, et al. C-Myb(+) erythro-myeloid progenitor-derived fetal monocytes give rise to adult tissue-resident macrophages. Immunity 2015;42:665–678.
[12] Sheng J, Ruedl C, Karjalainen K. Most tissue-resident macrophages except microglia are derived from fetal hematopoietic stem cells. Immunity 2015;43:382–393.
[13] Scott CL, Zheng F, De Baetselier P, Martens L, Saeys Y, De Prijck S, et al. Bone marrow-derived monocytes give rise to self-renewing and fully differentiated Kupffer cells. Nat Commun 2016;7:10321.
[14] Sierro F, Evrard M, Rizzetto S, Melino M, Mitchell AJ, Florido M, et al. A liver capsular network of monocyte-derived macrophages restricts hepatic dissemination of intraperitoneal bacteria by neutrophil recruitment. Immunity 2017;47, 374–388 e6.
[15] Han X, Wang R, Zhou Y, Fei L, Sun H, Lai S, et al. Mapping the mouse cell atlas by microwell-seq. Cell 2018;172:1091–1107 e17.
[16] Sanz E, Yang L, Su T, Morris DR, McKnight GS, Amieux PS. Cell-type-specific isolation of ribosome-associated mRNA from complex tissues. Proc Natl Acad Sci U S A 2009;106:13939–13944.
[17] Mohar I, Brempelis KJ, Murray SA, Ebrahimkhani MR, Crispe IN. Isolation of non-parenchymal cells from the mouse liver. Methods Mol Biol 2015;1325:3–17.
[18] Lynch RW, Hawley CA, Pellicoro A, Bain CC, Iredale JP, Jenkins SJ. An efficient method to isolate Kupffer cells eliminating endothelial cell contamination and selective bias. J Leukoc Biol 2018;104:579–586.
[19] Schaller E, Macfarlane AJ, Rupec RA, Gordon S, McKnight AJ, Pfeffer K. Inactivation of the F4/80 glycoprotein in the mouse germ line. Mol Cell Biol 2002;22:8035–8043.
[20] Gautier EL, Shay T, Miller J, Greter M, Jakubzick C, Ivanov S, et al. Gene-expression profiles and transcriptional regulatory pathways that underlie the identity and diversity of mouse tissue macrophages. Nat Immunol 2012;13:1118–1128.
[21] Abram CL, Roberge GL, Hu Y, Lowell CA. Comparative analysis of the efficiency and specificity of myeloid-Cre deleting strains using ROSA-EYFP reporter mice. J Immunol Methods 2014;408:89–100.
[22] Haimon Z, Volaski A, Orthgiess J, Boura-Halfon S, Varol D, Shemer A, et al. Re-evaluating microglia expression profiles using RiboTag and cell isolation strategies. Nat Immunol 2018;19:636–644.
[23] **Hagemeyer N**, **Kierdorf K**, **Frenzel K**, Xue J, Ringelhan M, Abdullah Z, et al. Transcriptome-based profiling of yolk sac-derived macrophages reveals a role for Irf8 in macrophage maturation. EMBO J 2016;35:1730–1744.
[24] Molawi K, Wolf Y, Kandalla PK, Favret J, Hagemeyer N, Frenzel K, et al. Progressive replacement of embryo-derived cardiac macrophages with age. J Exp Med 2014;211:2151–2158.
[25] Ginhoux F, Greter M, Leboeuf M, Nandi S, See P, Gokhan S, et al. Fate mapping analysis reveals that adult microglia derive from primitive macrophages. Science 2010;330:841–845.
[26] Epelman S, Lavine KJ, Beaudin AE, Sojka DK, Carrero JA, Calderon B, et al. Embryonic and adult-derived resident cardiac macrophages are

maintained through distinct mechanisms at steady state and during inflammation. Immunity 2014;40:91–104.
[27] Mizutani M, Pino PA, Saederup N, Charo IF, Ransohoff RM, Cardona AE. The fractalkine receptor but not CCR2 is present on microglia from embryonic development throughout adulthood. J Immunol 2012;188:29–36.
[28] Stremmel C, Schuchert R, Wagner F, Thaler R, Weinberger T, Pick R, et al. Yolk sac macrophage progenitors traffic to the embryo during defined stages of development. Nat Commun 2018;9:75.
[29] Van Rooijen N, Sanders A. Liposome mediated depletion of macrophages: mechanism of action, preparation of liposomes and applications. J Immunol Methods 1994;174:83–93.
[30] David BA, Rezende RM, Antunes MM, Santos MM, Freitas Lopes MA, Diniz AB, et al. Combination of mass cytometry and imaging analysis reveals origin, location, and functional repopulation of liver myeloid cells in mice. Gastroenterology 2016;151:1176–1191.
[31] Price JG, Idoyaga J, Salmon H, Hogstad B, Bigarella CL, Ghaffari S, et al. CDKN1A regulates Langerhans cell survival and promotes Treg cell generation upon exposure to ionizing irradiation. Nat Immunol 2015;16:1060–1068.
[32] Kuo LJ, Yang LX. Gamma-H2AX - a novel biomarker for DNA double-strand breaks. Vivo 2008;22:305–309.
[33] Purbey PK, Scumpia PO, Kim PJ, Tong AJ, Iwamoto KS, McBride WH, et al. Defined sensing mechanisms and signaling pathways contribute to the global inflammatory gene expression output elicited by ionizing radiation. Immunity 2017;47:421–434 e3.
[34] Teresa Pinto A, Laranjeiro Pinto M, Patricia Cardoso A, Monteiro C, Teixeira Pinto M, Filipe Maia A, et al. Ionizing radiation modulates human macrophages towards a pro-inflammatory phenotype preserving their pro-invasive and pro-angiogenic capacities. Sci Rep 2016;6:18765.
[35] Wu Q, Allouch A, Martins I, Modjtahedi N, Deutsch E, Perfettini JL. Macrophage biology plays a central role during ionizing radiation-elicited tumor response. Biomed J 2017;40:200–211.
[36] Georgakilas AG, Martin OA, Bonner WM. p21: a two-faced genome guardian. Trends Mol Med 2017;23:310–319.
[37] Brugarolas J, Chandrasekaran C, Gordon JI, Beach D, Jacks T, Hannon GJ. Radiation-induced cell cycle arrest compromised by p21 deficiency. Nature 1995;377:552–557.
[38] Abbas T, Dutta A. p21 in cancer: intricate networks and multiple activities. Nat Rev Cancer 2009;9:400–414.
[39] Koike M, Yutoku Y, Koike A. Accumulation of p21 proteins at DNA damage sites independent of p53 and core NHEJ factors following irradiation. Biochem Biophys Res Commun 2011;412:39–43.
[40] Chen W, Sun Z, Wang XJ, Jiang T, Huang Z, Fang D, et al. Direct interaction between Nrf2 and p21(Cip1/WAF1) upregulates the Nrf2-mediated antioxidant response. Mol Cell 2009;34:663–673.
[41] Baer K, Roosevelt M, Clarkson Jr AB, van Rooijen N, Schnieder T, Frevert U. Kupffer cells are obligatory for Plasmodium yoelii sporozoite infection of the liver. Cell Microbiol 2007;9:397–412.
[42] Bittmann I, Bottino A, Baretton GB, Gerbes AL, Zachoval R, Rau HG, et al. The role of graft-resident Kupffer cells and lymphocytes of donor type during the time course after liver transplantation–a clinico-pathological study. Virchows Arch 2003;443:541–548.
[43] **MacParland SA**, **Liu JC**, **Ma XZ**, Innes BT, Bartczak AM, Gage BK, et al. Single cell RNA sequencing of human liver reveals distinct intrahepatic macrophage populations. Nat Commun 2018;9:4383.